EVALUATION OF GEOTHERMAL ENERGY RESOURCES IN PARTS OF SOUTHEASTERN SEDIMENTARY BASIN, NIGERIA.

Okiyi, I.M.[1]; Ibeneme, S.I.[2]; Obiora, E.Y.[3]; Onyekuru, S.O[4]; Selemo, A.I.[5] and Olorunfemi, M.O.[6]

[1,2,3,4&5]Department of Geology, Federal University of Technology, Owerri Nigeria;
[6]Department of Geology, Obafemi Awolowo University, Ile-Ife, Nigeria,
(Corresponding Author: Okiyi, M.I; Email Address: millijey@yahoo.com)

ABSTRACT

Residual aeromagnetic data of parts of Southeastern Nigerian sedimentary basin were reduced to the equator and subjected to magnetic vector inversion and spectral analysis. Average depths of source ensembles from spectral analysis were used to compute depth to magnetic tops (Z_t), base of the magnetic layer (Curie Point Depth (CPD)), and estimate geothermal gradient and heat flow required for the evaluation of the geothermal resources of the study area. Results from spectral analysis showed depths to the top of the magnetic source ranging between 0.45 km and 1.90 km; centroid depths of 4 km - 7.87 km and CPD of between 6.15 km and 14.19 km. The CPD were used to estimate geothermal gradients which ranged from 20.3°C/km to 50.0°C/km and corresponding heat flow values of 34.9 mW/m^2 to 105 mW/m^2, utilizing an average thermal conductivity of 2.15 Wm^{-1}k^{-1}. Ezzagu (Ogboji), Amanator-Isu, Azuinyaba, Nkalagu, Amagunze, Nta-Nselle, Nnam, Akorfornor environs are situated within regions of high geothermal gradients (>38°C/Km) with models delineated beneath these regions using 3D Magnetic Vector Inversion, having dominant NW-SE and NE-SW trends at shallow and greater depths of <1km to >7 km bsl. Based on VES and 2D imaging models the geothermal system in Alok can be classified as Hot Dry Rock (HDR) type, which may likely have emanated from fracture systems. There is prospect for the development of geothermal energy in the study area.

Keywords: Airborne Magnetics, Magnetic Vector Inversion, Geothermal Gradient, Heat Flow, Curie Point Depth, Geothermal Energy.

INTRODUCTION

There is quest for the development of clean and renewable geothermal energy resources in developed and developing countries of the world, including Nigeria, as a means to sustainable power supply and economic growth. Geothermal energy can also be developed as an alternative to fossil fuel, thereby reducing the global environment impact of fossil fuelling. Nigeria is recognized as one of the African countries with potential for geothermal energy (IGA, 2020). Surface manifestations of subsurface heat as springs and lava flow have been reported in both the sedimentary and the Precambrian Basement Complex areas of Nigeria. As observed by Abraham and Nkitnam (2017), eight (8) out of the ten (10) well known thermal or warm springs in Nigeria are situated in the Northern and Central portions of the Cretaceous Benue Trough. These include Lamurde Hot Spring, Keane-Awe Thermal Springs, Akiri Warm Spring and Wikki Warm Spring with recorded water temperatures of between 32°C and 54°C. Rafin Rewa Warm Spring and the Ikogosi Warm Spring are situated in migmatite gneiss and fractured quartzite schist Precambrian Basement rocks respectively with water temperatures of 42.5°C and 37°C.

The down-dip part of the Nigerian sector of the Eastern Dahomey (Benin) Basin, in the Southwest, is also suspected to have high potential for geothermal energy development. Two boreholes drilled to depths of 500 m - 522 m by OAK Group of Companies at Isheri area of Ogun State, Nigeria, discharge warm free-flowing groundwater with temperatures of 55°C – 65°C. Also, boreholes drilled at Ikeja and Ikorodu areas of Lagos State to depths of 760 m and 650 m within the Coastal Plain Sands also discharge groundwater with temperatures of 72°C and 59°C respectively (OAK GROUP, 2013). Geothermal energy is a huge reservoir of thermal energy in the earth's interior whose surface manifestations are volcanoes, fumeroles, geyseys, steaming grounds and warm/hot springs (Shah *et al.,* 2015)

The Earth's inner temperature can be measured in the immediate vicinity of the Earth's surface, in

boreholes and deep mines based on warmer conditions in it (Hoover and Hoover, 1556). Near-surface temperatures increase rapidly with depth by roughly 30 Kkm^{-1} and at this rate, linear extrapolation would yield a temperature of 200,000 K at the center of the Earth. As a result of the earth's heat flow constantly from the earth to the surface, total heat loss from the Earth is estimated at 44.2 TW, mean heat flow at 65 mW/m^2 over continental crust and 101 mW/m^2 over oceanic crust (Perry, 1895a-c). The global geothermal flow rates are more than twice the rate of human energy consumption from all primary sources, indicating the enormous resource of geothermal energy. Heat increase in the earth causes temperature to rise by an amount (dT), determined by the specific heat at constant pressure (cp) and the mass of material (m) in the earth (Lowrie, 2007) which explains the geothermal gradient. Away from tectonic plate boundaries, it is about 25 °C per km of depth (1 °F per 70 feet of depth) near the surface in most of the world (Beardmore and Cull, 2001). Heat below the surface is relatively constant and it denotes heat from earth's interior, also supplemented with subsurface oxidation and other local heat sources which establishes the rock temperature below the zone where the effect of surface temperature is perceptible (Lovering and Goode, 1963 and Donny *et al.*, 2020). Increased geothermal gradient is a lot useful in several geological processes such as kerogene maturation, geothermal reserve accumulation for electricity generation, ore-fluid migration, accretion and mineral precipitation. Steep temperature gradients are responsible for oxidizing sulphides at depth and these anomalous gradients are helpful in searching blind ore bodies (Lovering and Goode, 1963). Increasing both temperature and pressure during burial triggers a series of mineral reactions and phase changes that may release water and ions in carbonate diagenetic processes. For example, the conversion of gypsum to anhydrite at about 1000 m releases significant water that may become involved in solution, cementation or dolomitization (Kendall, 1984). Aside this, elevated temperatures over extended period of time, lead to catagenesis of organic compounds and formation of oil and gas (Tissot and Welte, 1978). Such is observed in shales of Maamu and Nkporo Formations in Enugu, which are rich in coal deposits derived from terrestrial organic matter from brackish marsh and fossiliferous pro-delta facies of late Campanian to early Maastrichtian depositional cycle (Reijers and Nwajide, 1998), about 70 Ma.

The Lower Benue Trough (LBT), which contains the study area, is a tensional feature and a rift structure within the Benue Trough (aulacogen/failed rift) which resulted from proto-rifting of boundary area between South American and African plates at a triple R (RRR) junction, under present day Niger Delta (Petters, 1978). Continuous movement along Atlantic spreading ridge and faults of the ridge offset resulted in physiographic and structural dispositions with the spread halting at the late Cretaceous basin. The over 800 km long intra-continental Benue Trough which trend NNE–SSW, and about 150 km wide, was initiated during the lower Cretaceous in relation to the rifting, leaving heavily silted, compressed, folded, faulted, and uplifted Cretaceous-Tertiary sediments >5000 m within pre and mid Santonian times. The overpressured thick sediment strata have remarkably generated regions of anomalous temperature gradients, which have influenced heat flow. There are surface manifestations of the geothermal heat as warm and hot springs in the central and northern parts of the Benue Trough (Abraham and Nkitnam, 2017). The geothermal energy potential of LBT is yet to be assessed, hence this study.

Exploration for geothermal energy often involves geological (including remote sensing), geophysical and geochemical investigations (El-Qady, 2006; Kana *et al.*, 2015; Shah *et al.,* 2015; Chabaane *et al.,*2017; Azaiez *et al.,* 2020), Geophysical investigation is either direct, involving methods that measure parameters (e.g. temperature, fluid content, resistivity/conductivity) that are directly influenced by geothermal activity such as the thermal, electrical resistivity, magnetotelluric (electromagnetic) and self-potential methods or indirect with methods that explore the physical parameters of the host rock (e.g. magnetic property, density, seismic velocity) that enable the mapping of subsurface structures or geological bodies including the magnetic, gravity and seismic reflection methods (Georgsson, 2013; Shah *et al.*, 2015).

In Nigeria, geoelectrical and magnetic (ground and airborne) methods are commonly adopted (Ojo *et al.,* 2011 and Abraham *et al.*, 2011). Regional aeromagnetic data are used to determine the bottom of the magnetic portion of the crust and to map the Curie isotherm surface. High heat flow and geothermal gradients constituting thermal anomalies are good geothermal energy reserves. The regional distribution of thermal anomalies in the crust is controlled by regional tectonic patterns. This study evaluates the potential of geothermal energy in the study area using anomalous heat flow and geothermal gradients by engaging high resolution aeromagnetic data.

Description of the Project Area
Geographic Location, Drainage, Vegetation and Climate
The study area is the Southeastern Nigerian sedimentary basin of the Lower Benue Trough (LBT) which covers the States of Anambra, Enugu, Ebonyi, Imo, Abia, Akwa Ibom and Cross River. It is located between Latitudes 5° 30' N and 7°00' N and Longitudes 7° 00' E and 9° 00' E (Figure 1). It is bounded by Kogi State to the North, Delta and Edo to the West and Bayelsa and Rivers States to the South; and to the East by the Cameroon. There is a dendritic pattern of drainage in the area linked to various tributaries of the Cross River. Discontinued river channels are prompted by seasonal variations usually from harmattan and August break of the dry seasons which interrupt the distribution of rivers in these tributaries. The vegetation is the ever green type composed of eastern prototype mixtures of semi-savannah grasslands, forests and swamps. An average annual rainfall precipitation of >3000 mm typifies a rainforest environment and influences the vegetation type (Okiyi *et al.*, 2021).
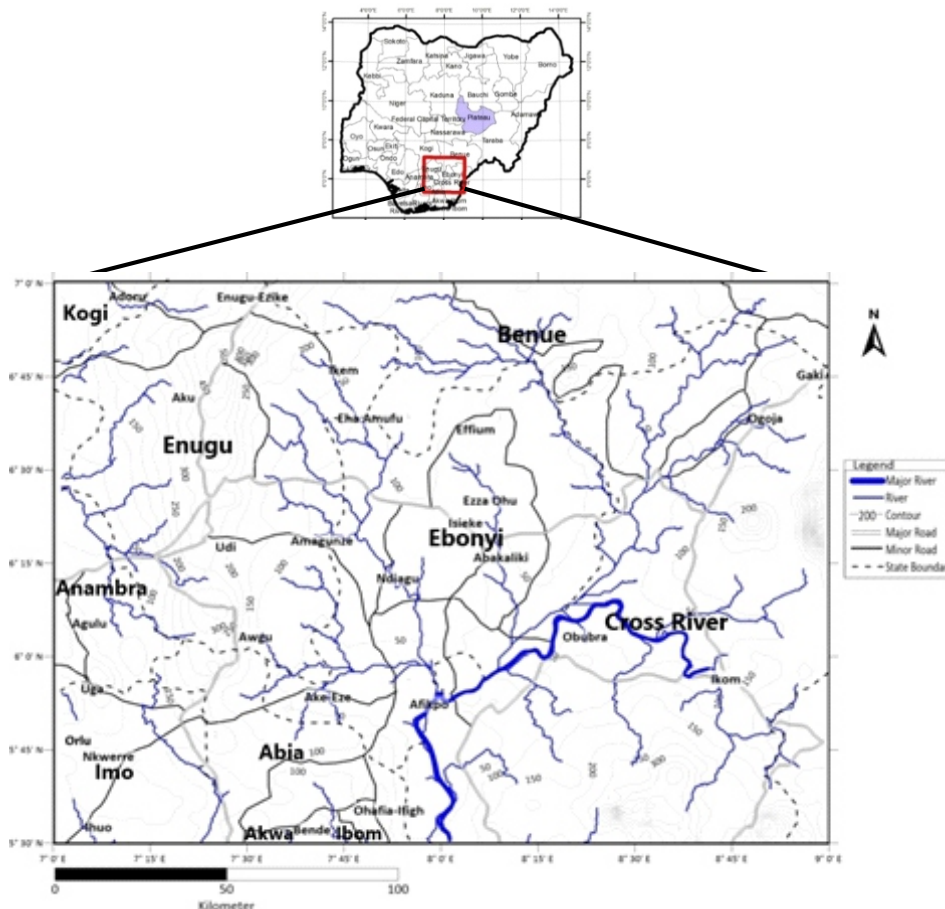

Figure 1 Topographical map of the study area (Digitized from Ryan *et al.*, 2009 and Adapted from Okiyi *et al.,* 2021)

Regional Tectonic Setting and Geology

The southeastern Sedimentary Basin is part of a tensional feature and the Benue Trough rift structure, which started at a triple R (RRR) junction, under present day Niger Delta. At that time, Gulf of Guinea, Benue depression and the South Atlantic developed between two of the triple Rs North of the junction, one between South America and along Niger Delta (Petters, 1978). Continuous movement along the Atlantic spreading ridge and faults within the ridge offset resulted in physiographic and structural disposition. The area covered by the present day Benue valley was also spreading. But separation and sea floor spreading in the Benue Trough stopped at late Cretaceous. Lately, activities started along the Cameroon plate which has many embryonic spreading ridge. Intracontinental Benue Trough was initiated during the lower Cretaceous in relation with the Atlantic Ocean opening. The Benue Trough extends NNE–SSW for about 800 km in length and 150 km in width. The southern limit is the northern boundary of the Niger Delta, while the northern limit is the southern boundary of the Chad Basin. The Trough contains up to 6,000 m of Cretaceous-Tertiary sediments of which those predating the mid-Santonian have been compressionally folded, faulted, and uplifted in several places. Compressional folding during the mid-Santonian tectonic episode affected the whole of the Benue Trough and was quite intense, producing over 100 anticlines and synclines (Benkhelil, 1989). Major deformational structures include the Abakaliki Anticlinorium and the Afikpo Syncline in the Lower Benue Trough.

The study area hosts both sedimentary strata and igneous structures and most igneous structures resulted from magma pluming into the Cretaceous riftogenic sediments. The first transgressive cycle of Neocomian-Albian marine Asu River Group sediments are massively sustained from shales, localized sandstones, siltstones, limestones and magmatic intrusives/extrusives of Alptian-Albian and the Mfamosing Formation in the Calabar flank consisting of folded basement rocks (Obaje, 2009). This formation is overlain by the Cenomanian-Turonian transgressive sediments of Ezeaku Formation and Coniacian to pre-Santonian Awgu shales (Ladipo, 1988; Akande *et*

al., 1992 and Nwajide, 2013) having unified occurrences of fine-grained carbonaceous limestone beds, limestone, calcareous sandstones and interfingering regressive sandstones of the Agala and Agbani Formations. In sync to the Nkalagu Formation separated by episodes of unconformities, was silting sequence of sandstones, limestones, shales and calcareous sandstones of Odukpani Formation. Succeeding the afore-mentioned formations is the Campanian-Paleocene post-Santonian sediments of the Anambra Basin. The Santonian hiatus was encumbered in compressive forces which originated dominant NE-SW folds and synclines (Obaje, 2009). Displacement of the geo-pressured depo-centre westward, led to the formation of post-deformational sequences in the LBT, constituting Anambra Basin (Odoma *et al.,* 2013 and Nwajide, 2013). Sediments of the third marine transgressive cycles commenced sedimentation in this basin, which span from bluish to dark grey shales, sandy shales, thin sandstones and shaly limestone beds, all constituting the pro-delta facies of the Campanian-Early Paleocene. The lower Imo Shale alongside Upper Nsukka Formation, marks a minor regression and onset of another Paleocene transgression in the Anambra Basin. Tidal Nanka Sandstone of Agbada Formation initiates a return to regressive conditions as seen from predominant flood-tidal currents (Fatoye *et al.*, 2014). Prominent basins such as Anambra, Afikpo, Mamfe and Niger Delta Basins alongside the afore-detailed Paleozoic to Eocene formations, are contained in the study area as elaborated in the geologic map below (Figure 2a). Sediments of the Anambra Basin are obviously thickest and most silted up >450 m asl (Figure 2b).

MATERIALS AND METHOD OF STUDY

Materials

This study utilized airborne magnetic data acquired from the Federal Ministry of Mines and Steel Development, Nigeria, between 2005 and 2009 through Fugro Airborne Surveys Limited. The high resolution data were acquired with 500 m line spacing and 80 m terrain clearance for most parts of Nigeria. Subsequently, these data were divulged by the Nigerian Geological Survey Agency (NGSA) in 2010. Twelve (12) data sheets which include Nsukka 287, Igumale 288, Ejekwe

289, Ogoja 290, Udi 301, Nkalagu 302, Abakaliki 303, Bansara 304, Okigwe 312, Afikpo 313, Ugep 314, and Ikom 315 were obtained from the aforementioned government agency. The aeromagnetic data were geo-referenced to the Universal Transverse Mercator coordinate system, to make effective comparison with other digitized maps of the area.

Method of Study
Aeromagnetic Data Enhancement Routines
(a) Reduction to Equator (RTE)
The acquired residual Total Magnetic Intensity (TMI) data were reduced to the magnetic equator (RTE) to minimize polarity effects by applying the parameters: Longitude: 7.5°, Latitude: 5.5°, Inclination: -15.82788831, Declination: -1.63207023 and IGRF model: 2015/08/15. This generally corrects for secular and transient variations within the survey area and ignores that change in the intensity of induced magnetic anomalies is due to change of inducing magnetic field. The corrections are usually applied as well to remove magnetic field effects, caused by the aircraft (Korhonen, 2005).

(b) Magnetic Vector Inversion
The 3D magnetic vector inversion (MVI) of geomagnetic field data is an advanced technique used in quantitative interpretation of the magnetic data because it extrapolates property and geometry of subsurface magnetic structures in 3D using subsurface magnetic susceptibility from observed magnetic data (Utsugi, 2019).The anomalous magnetic field vector projected into the inducing field direction is expected to approximate total field anomaly. MVI uses 3D distribution of magnitude of magnetization, dependent on both direction and magnitude and obtained through inversion (Li, 2017) as shown below:

$$\Delta \text{T}(\vec{r}) = \frac{\mu_0}{4\pi} \iiint_v^v \text{J}(\vec{r}')\hat{\jmath}(\vec{r}') \cdot \nabla^T \nabla \frac{1}{|\vec{r}-\vec{r}'|} \hat{B}_0 \, \text{d}v' \qquad (1)$$

Where J = magnetic polarization, $\text{J}(\vec{r})$= magnitude and $\hat{\jmath}$ = unknown direction and $\hat{\jmath}=\hat{B}_0$ assuming weak magnetization for susceptibility magnetization. This distribution pre-requires inversion of amplitude data to equal length of anomalous magnetic field vector and recovering magnetization as:

$$B_a=|B_a| = \sqrt{B^2ax + B^2ay + B^2az}$$
(Shearer, 2005; Li *et al*, 2010) $\qquad (2)$
where B_a = amplitude; B_{ax}, B_{ay} and B_{az} = three orthogonal components of the magnetic anomaly vector.

The DSIM3D is a Geosoft GX implementation of an inversion approach (Pilkington, 2009) in OASIS Montaj environment that determines 3D susceptibility distribution from input magnetic anomaly data. The GX accepts gridded magnetic data as input and produces a subsurface 3D model of the magnetic susceptibilities of an equally spaced array of dipoles. DSIM3D provides a rapid, unconstrained 3D inversion of gridded magnetic data. The original inversion software DSIM3D was written as a FORTRAN code (Pilkington, 2009). A Geosoft GX implementation of the original code is presented. The inversion involves depth weighting of the solution and is posed in the data space, leading to the linear system of equations with dimensions based on the number of data, N. This contrasts with the standard least-squares solution derived through operations within data space method combined with a conjugate gradient algorithm leads to computational efficiency by dealing with an N×N system versus an M×M where N<<M. (Pilkington and Bardossy, 2015).

(c) Spectral Analysis, Curie Point Depth, Geothermal Gradient and Heat Flow
Surface magnetic field is considered an integral of magnetic signatures from all depths which is the principle behind the spectral depth method. The average depth of source ensembles is identified by power spectrum of the surface field (Spector and Grant, 1970), which is the logarithm of the power of the signal at each wavelength plotted against wavelength, regardless of direction. The power spectrum is observed to be series of broken up straight line segments where each line segment represents cumulative response of a discrete ensemble of sources at a given depth and the depth is directly proportional to the slope of the line segment. This is a reliable technique to identify characteristic depth of the magnetic basement. The radial average spectrum was performed using the Oasis Fast Fourier Transform (FFT) routine in frequency domain which converts RTE-TMI data from spatial to frequency domain.

Depth to the top of magnetized rectangular prisms (Z_t) was estimated by Spector and Grant (1970) from the slope of log power spectrum. Bhattacharyya and Leu (1975 a&b) further calculated the depth of the centroid of the magnetic source bodies (Z_0). Okubo *et al.* (1985) developed the method to estimate the bottom depth of the magnetic bodies (Zb) using the spectral analysis method of Spector and Grant (1970). Tanaka *et al.* (1999) assumed that the layer extends infinitely in all horizontal directions. The depth to a magnetic source's upper bound is much smaller than the magnetic source's horizontal scale, and the magnetization M(x, y) is a random function of x and y, hence Blakely (1995) introduced the power-density spectra of the total-field anomaly$\emptyset_{\Delta T}$ (Hsien-Hsiang *et al.,* 2014) as defined below:

$$\emptyset_{\Delta T}(k_{x1}, k_y) = \emptyset_M(k_{x1}, k_y) \times F(k_{x1}, k_y) \quad (3)$$

$$F(k_x, k_y) = 4\pi^2 C_m^2 |\theta_m|^2 |\theta_f|^2 e^{-2|k|z_t}(1 - e^{-|k|(z_b - z_t)})^2 \quad (4)$$

$\emptyset_M$ = Power–density spectra of the magnetization, θ_m and θ_f = factors for magnetization, C_m = proportionality constant, $|\theta_m|^2$ and $|\theta_f|^2$ are radially symmetric and the variables are constant, if M(x, y) is random and uncorrelated, $\emptyset_M(k_{x1}, k_y)$ is a constant.

$$\emptyset_{\Delta T}(|k|) = Ae^{-2|k|z_t}(1 - e^{-|k|(z_b - z_t)})^2 \quad (5)$$

A = constant and k = wavenumber. For wavelengths less than about twice the thickness of the layer:

$$\ln\left[\emptyset_{\Delta T}(|k|)^{\frac{1}{2}}\right] = \ln B - |k|Z_t \quad (6)$$

If B = constant, the upper boundary of a magnetic source Z_t by line of best fit through high wave number part of a radially averaged power spectrum $\ln\left[\emptyset_{\Delta T}(|k|)^{\frac{1}{2}}\right]$

$$\emptyset_{\Delta T}(|k|)^{\frac{1}{2}} = Ce^{-|k|z_0}(e^{-|k|(z_t - z_0)} - e^{-|k|(z_b - z_0)}) \quad (7)$$

where C = constant. At long wavelengths;

$$\emptyset_{\Delta T}(|k|)^{\frac{1}{2}} = Ce^{-|k|z_0}(e^{-|k|(-d)} - e^{-|k|(d)}) \approx Ce^{-|k|z_0} 2|k|d \quad (8)$$

For 2d thickness of the magnetic source, it can be

concluded that:

$$\ln\left[\frac{\emptyset_{\Delta T}(|k|)^{\frac{1}{2}}}{|k|}\right] = \ln D - |k|Z_0 \quad (9)$$

D = constant. The centroid of the magnetic source Z_0 is estimated by fitting a straight line through the low wavenumber part of the radially averaged frequency-scaled power spectrum

$$\ln\left[\frac{\emptyset_{\Delta T}(|k|)^{\frac{1}{2}}}{|k|}\right]$$

The slope of the power spectrum calculates the top boundary (Z_t) and the centroid of magnetic sources (Z_o) which in turn is used to estimate the bottom depth/Curie point depth (Z_b) of the magnetic source using the relation;

$Z_b = 2Z_o - Z_t$ (Spector and Grant, 1970; Okubo *et al.*, 1985 and Tanaka *et al.*, 1999) (10)

In relating the Curie point depth (Z_b) to Curie point temperature (580°C), vertical direction of temperature variation and constant thermal gradient were assumed. The geothermal gradient (dT/dz) between the Earth's surface and the Curie point depth (Z_b) was estimated using the equation:

$$GG = \frac{dT}{dZ} = \frac{\theta_c}{Z_b} \quad \text{(Tanaka *et al.* (1999); Stampolidis *et al.*, 2005; Maden, 2010) (11)}$$

Where θ = 580°C (Curie Temperature). Heat flow (mW/m^2) was estimated using the relation;

$$q = K\left(\frac{dT}{dz}\right) = \lambda\frac{\theta_c}{Z_b} \quad \text{(Turcotte and Schubert, 1982;}$$
Tanaka *et al.*,1999): (12)
where k = 1.8 and 2.5 Wm^{-1}c^{-1} for sedimentary and igneous rock formations and λ = coefficient of thermal conductivity.

A 55 x 55 km window dimension was used with 50% overlapping data window (Figure 3) selected for spectral analysis procedures on the RTE-TMI map. The region of probe is the center of the window which was done by taking the diagonals of the rectangle alongside actual points of intersection, with assumption that it is a rectangular window. The coordinates of these points were taken for the cartesian but numbers were taken for linear plots. Windows around regions of mixed/active anomaly regions were zeroed in and restricted to obtain results. A depth solution was calculated and power spectrum derived from each grid sub-set located at center of the window. Overlapping the windows creates a regular, comprehensive set of depth estimates

which can be automated, with limitation of having least squares best-fit straight line segment always calculated over the same points of the power spectrum. Two (2) spectral plots from the first two blocks out of 35 blocks sampled were used as case study. For this window size/dimension taken, just half of the window gets probed, computing the depth of the spectra and estimating the Curie Point Depth (CPD) using equation 13;

Depth of Spectra $= \frac{L}{2\pi}$ (Sheuy *et al.*,1997 & Ravat *et al.,* 2007)   (13)

 where L = Length of the window/Dimension of block.

(d) Vertical Electrical Sounding and 2D Imaging Beneath Areas of Anomalous Geothermal Gradients

Schlumberger array was used in 2D imaging from two 500 meters perpendicular traverses at areas of high geothermal gradient, precisely Alok and Amagunze. However, Alok is used as a case study to investigate the influence of fracture system as pathway to heatflow. The current electrode spacings AB/2, were varied from 2 to 3, 6, 9, 15, 25, 40, 50, 75, 100, 150, 200, 300, 400 and 500 meters at both sides from the centre point making a total of 1 km along both traverses. The potential electrodes spacings (AB/2) were expanded at both sides from the center point at 0.5, 2.0, 10 and 20 meters. Repeated readings were done at same current electrode spacings of 9, 75, 300 meters where potential electrodes were expanded to allow increased and measurable potential difference. The product of the geometric factor (G) (equation 14) for Schlumberger array and true resistance gave the apparent resistivity values which were plotted against electrode separation AB/2 (m) to obtain field curves. Resistivity and thickness values of geoelectric layers gotten from

direct and automated iteration of the resistivity curves, yielded geoelctric sections from which subsurface images were obtained using RES2D Inversion software.

Geometric factor (G) $= \frac{\pi[l^2 - b^2]}{2b}$ (14)
where l=   distance of current electrodes from center point and b = distance of potential electrodes from the center point.

## RESULTS AND DISCUSSION

Evaluation of Anomalous Geothermal Gradients and Appraisal of the Influence of Structures

Various ranges of values representing varying degrees of magnetizations on the RTE-TMI map are categorized as: very low for -45.9 to 14.5 (nT) in by blue; low for 14.7 to 51.35 (nT) in green; average for 54 to 59 (nT) in green; moderate for 64.5 to 87 (nT) by brown to dark orange and high for 94.2 to 121.7 (nT) in red. Very high magnetic responses >120 nT are displayed in red to purple colour. High magnetic intensities are seen basically in the South and Northwestern parts of the study area. Elliptical contours represent isolated high magnetic anomalies, depicting near-surface responses of buried bodies, mainly intrusive structures (Akanbi and Udensi, 2006). Near-surface intrusives are likely prevalent in Umuahia and Okigwe as seen from high magnetic reliefs >120nT, which show a general E-W and NE-SW trends in Okigwe, Afikpo, Udi, Obudu, Okposi, Obubra, Apiapum e.t.c. The basement is characterized by low magnetic relief anomalies on RTE-TMI map (Fig. 3), with low magnetic closures depicting faulted zones. Reynold *et al.*, 1990 and Opara, 2011 have also attributed series of low magnetic closures to linear trends, which initiate shear/fault zones.
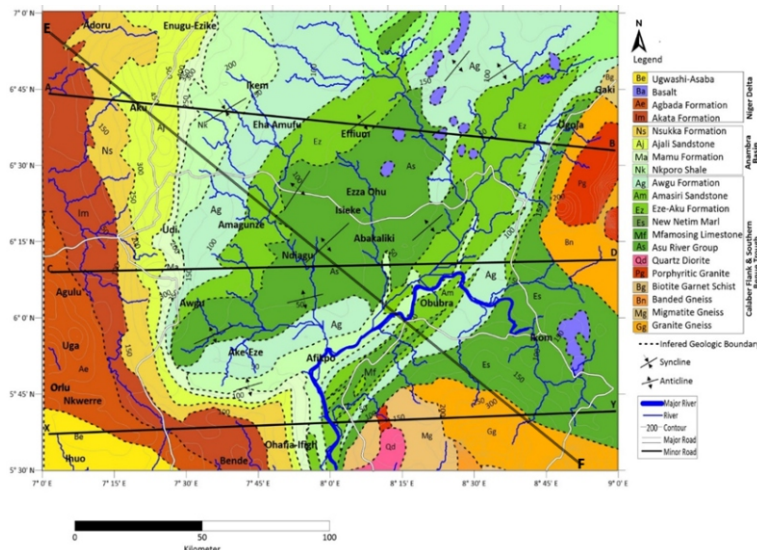
(Fig. 2a)

Figure 2a Geologic Map (Digitized from geologic map of Nigeria, NGSA, 2010) with profile lines
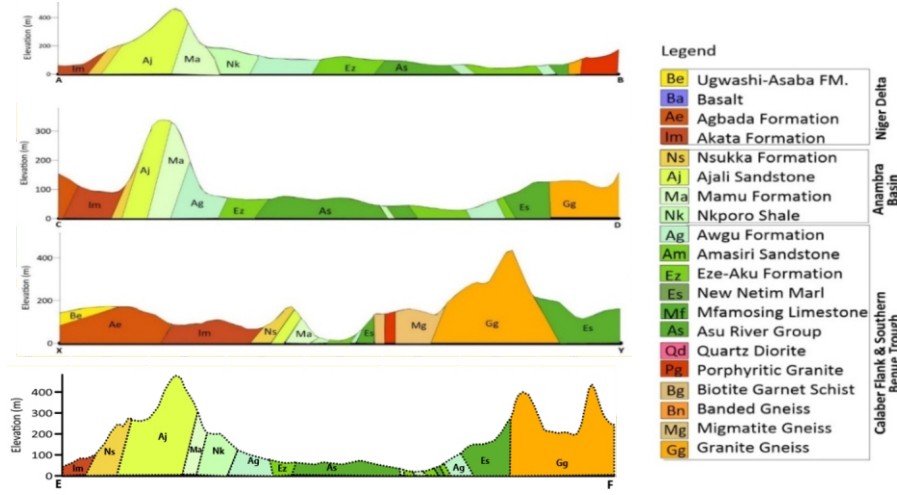
(Fig. 2b)

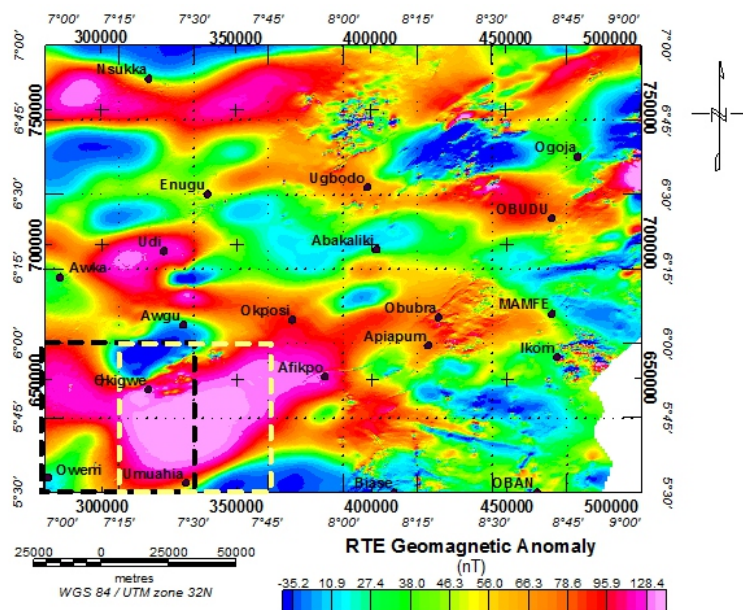Figure 2b Geological cross-sections obtained across the profile lines

Figure 3 55×55 km windowed on RTE- Geomagnetic anomaly map

Table 1: Spectral Analysis results for 35 Windows of 55 x 55 km dimension and 50% overlap. The respective uncertainty of each window was also evaluated

| Block	Location		z_t (km)	Error z_t ($\pm$ km)	z_o (km)	Error z_o ($\pm$ km)	CPD (km)	Error CPD ($\pm$ km)	GG(°C/km)	Heat Flow (mW/m2)	Geologic Formation
	Longitude (°)	Latitude (°)									
1	7.25	5.75	1.378	0.078	7.514	0.272	13.65	1.76	18.69084249	33.64351648	Agbada shales
2	7.5	5.75	1.889	0.318	7.257	0.254	12.63	3.01	22.12240697	39.82033255	Ajali Sand St.
3	7.75	5.75	1.558	0.095	7.874	0.256	14.19	1.79	17.07385483	30.73293869	Mamu Fm
4	8	5.75	1.108	0.024	6.531	0.27	11.95	1.24	24.73556485	44.52401673	Amaseri Sand St.
5	8.25	5.75	0.69	0.073	5.974	0.253	11.26	2.14	27.70976909	46.72710623	migmatite gneiss
6	8.5	5.75	0.94	0.107	5.568	0.238	10.2	2.03	33.0627451	55.30601743	granite gneiss
7	8.75	5.75	0.441	0.052	4.259	0.014	8.08	1.01	47.98217822	86.3679208	new netim marl
8	8.75	6	0.824	0.081	5.708	0.225	10.59	1.88	30.96864967	55.74356941	Awgu shale
9	8.5	6	0.578	0.026	6.597	0.281	12.62	1.64	22.15879556	39.88583201	Awgu shale
10	8.25	6	0.451	0.034	4.864	0.022	9.28	0.79	38.7	69.66	Nkporo shale
11	8	6	1.377	0.069	5.271	0.014	9.17	0.51	39.44972737	71.00950927	Awgu shale
12	7.75	6	1.51	0.067	4.747	0.019	7.98	0.42	48.88170426	87.98706767	Asu River G
13	7.5	6	1.28	0.018	5.499	0.012	9.72	0.18	35.87078189	64.5674074	Asu River G
14	7.25	6	1.257	0.062	6.334	0.274	11.41	1.55	27.03260298	48.65868536	Imo shale
15	7.25	6.25	1.158	0.138	5.106	0.021	9.06	1.15	40.21766004	72.39178807	Imo shale
16	7.5	6.25	1.185	0.088	5.199	0.018	9.21	0.75	39.17502714	70.51504885	Awgu shale
17	7.75	6.25	1.529	0.015	4.296	0.092	7.06	0.37	58.3529745	105.0353541	Ezeaku Shale
18	8	6.25	1.124	0.034	5.233	0.133	9.34	0.76	38.29850107	68.93730193	Asu River G
19	8.25	6.25	0.997	0.017	7.554	0.277	14.11	1.27	17.30559887	31.15007797	Asu River G
20	8.5	6.25	1.102	0.063	3.626	0.091	6.15	0.66	60.50894309	108.9161000	Ezeaku Shale
21	8.75	6.25	1.122	0.089	4.482	0.199	7.84	1.32	50.17959184	110.3951000	Banded gneiss
22	8.75	6.5	0.712	0.027	4.464	0.113	8.22	0.73	46.75961071	84.16729928	Ezeaku Shale
23	8.5	6.5	0.654	0.016	5.609	0.029	10.57	0.36	31.07228004	55.93010407	Ezeaku Shale
24	8.25	6.5	0.657	0.028	4.611	0.026	8.56	0.46	43.95700935	79.12261683	Asu River G
25	8	6.5	0.584	0.037	4.528	0.016	8.47	0.59	44.67697757	80.41855963	Asu River G
26	7.75	6.5	0.682	0.018	4.001	0.175	7.32	0.83	55.43497268	99.78295082	Awgu shale
27	7.5	6.5	1.502	0.062	5.118	0.141	8.73	0.84	42.63757159	76.74762886	Nkporo shale
28	7.25	6.5	1.849	0.118	5.873	0.033	9.89	0.74	34.84509606	62.72117291	Nsukka Fm
29	7.25	6.75	1.372	0.128	7.137	0.073	12.9	1.47	21.16124031	38.09023256	Nsukka Fm
30	7.5	6.75	1.604	0.135	7.134	0.08	12.66	1.35	22.0135861	39.62445498	Maamu Fm
31	7.75	6.75	1.098	0.022	6.649	0.081	12.2	0.54	23.74098361	42.7337705	Nkporo shale
32	8	6.75	0.628	0.024	5.466	0.037	10.3	0.53	32.51067961	58.5192233	Awgu shale
33	8.25	6.75	0.68	0.029	5.587	0.027	10.49	0.56	31.4907531	56.68335558	Awgu shale
34	8.5	6.75	0.698	0.023	5.857	0.039	11.02	0.52	28.83157895	51.89684211	Ezeaku Shale
35	8.75	6.75	0.797	0.034	5.079	0.026	9.36	0.5	38.16581197	68.69846155	Ezeaku Shale
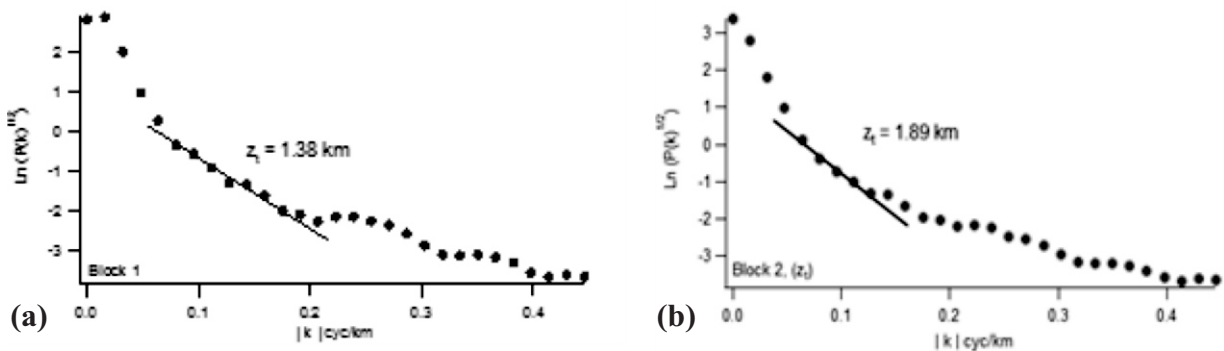
Figure 4a&b   Spectral plots for the 55 x 55 km windows taken across the study area used to compute depths to the top of magnetic sources.
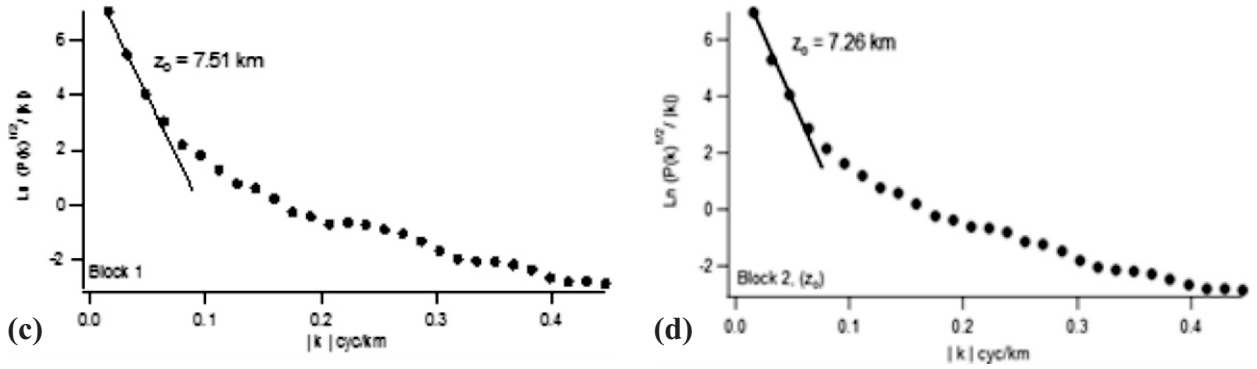
Figure 4c&d   Spectra plots utilized to compute depths to the centriod of magnetic sources in the region.
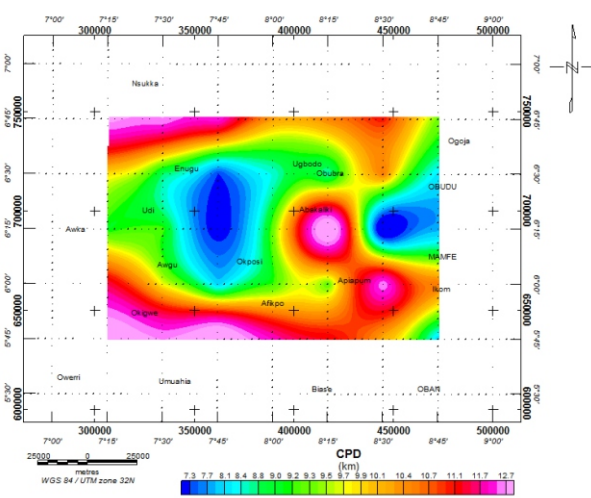

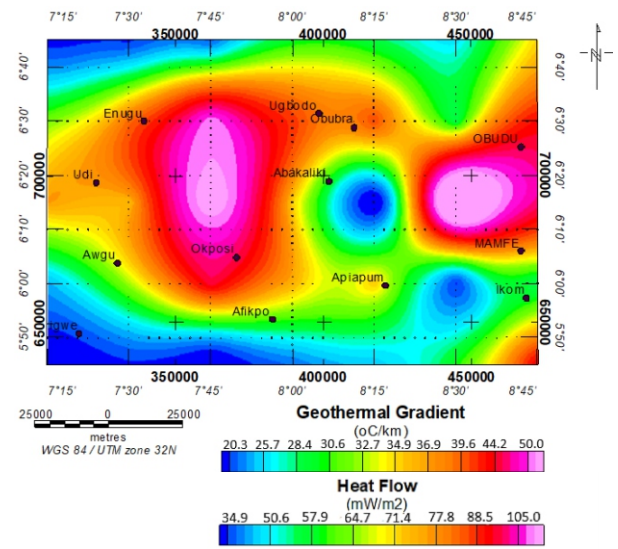Figure 5a   Map representation of the computed Curie Point Depths

Figure 5b   Geothermal gradient (GG) map computed from derived CPD data.
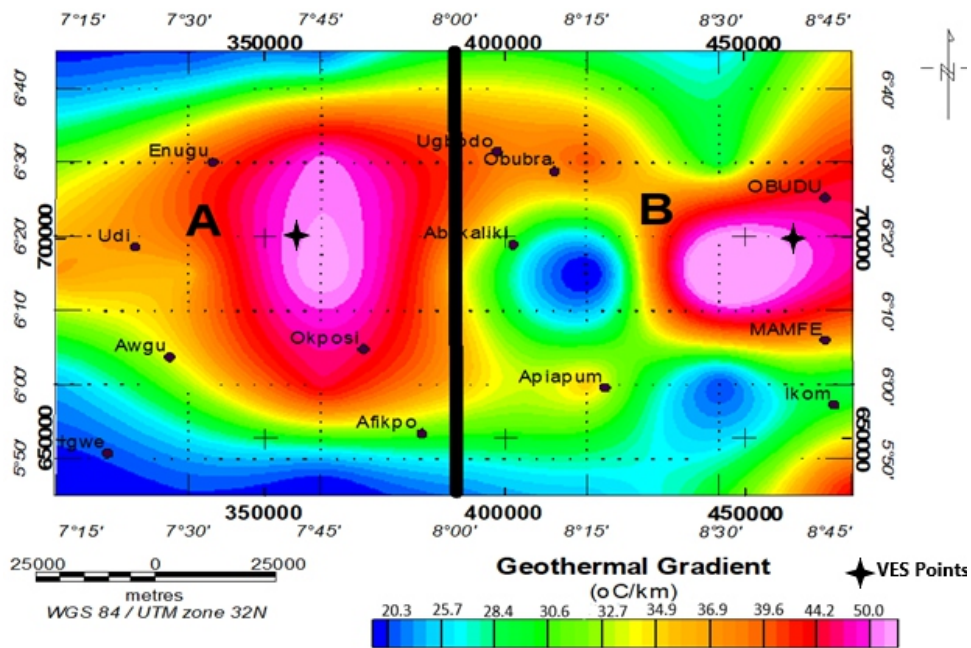

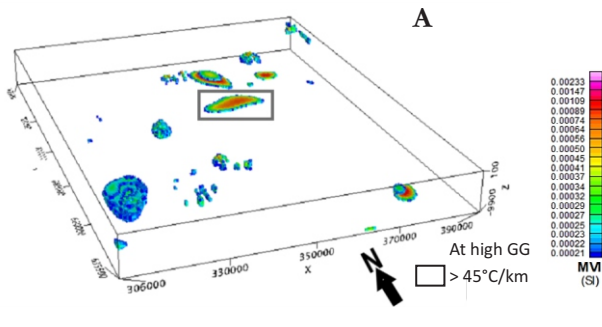Figure 6 Geothermal gradient map sectioned into parts A and B with VES Points

Figure 7a Subsurface imaging results from part A of the geomagnetic anomaly field data covered in 55 x 55 km window
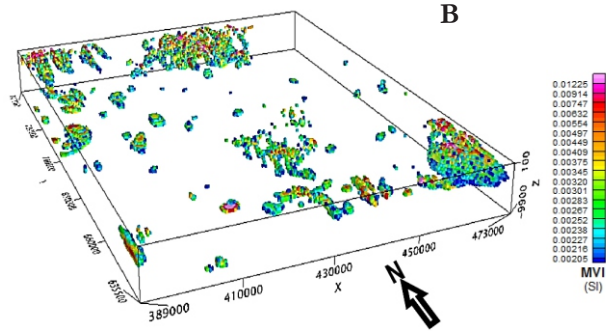

Figure 7b Subsurface imaging results from part B of the geomagnetic anomaly field data covered in 55 x 55 km window
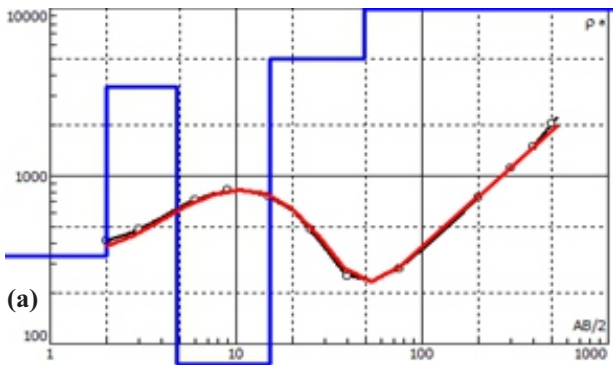

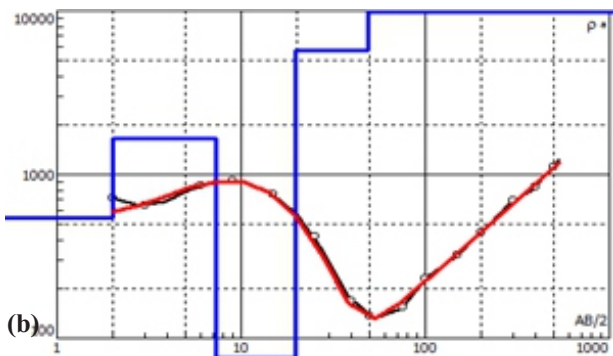| Nnam Alok: Traverse 1 -Nnam Alok Comp. Sec. School				
Curve type: KH Type-$\rho_{1<}\rho_2 > \rho_3 < \rho_4 < \rho_5$				
Layers	Lithology	ρ_a(Ωm)	Thickness(m)	Depth (m)
1.	Laterized sand	334	2.01	2.01
2.	Lateritic shale	3391	2.84	4.85
3.	Fractured clay	41.1	10.3	15.1
4.	Partly weathered/ Fractured Basement	4977	33.6	48.7
5.	Undifferenciated basement	63540	?	?

Figure 8a Evaluation of geoelectric layers from Nnam Alok VES data along Traverses 1

Nnam Alok: Traverse 2 -Akorfornor-Ogomogo				
Curve type: KH Type-$\rho_{1<}\rho_2 > \rho_3 < \rho_4 < \rho_5$				
Layers	Lithology	ρ_a(Ωm)	thickness	depth
1.	Weathered basement	547	2.01	2.01
2.	Lateritic shale	1659	5.36	7.36
3.	Fractured clay	27.9	12.2	19.6
4.	Partly weathered /Fractured Basement	5734	29.1	48.7
5.	Undifferenciated basement	64316		

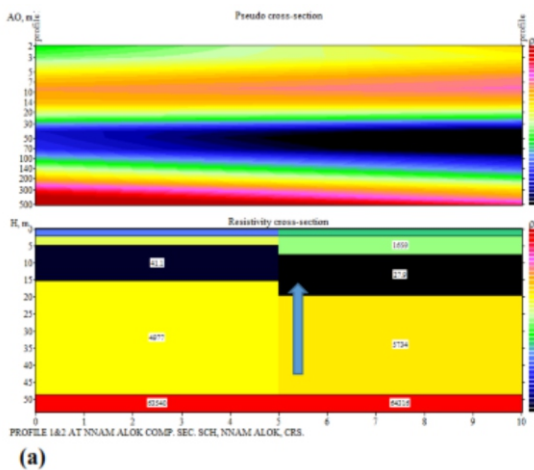Figure 8b Evaluation of geoelectric layers from Nnam Alok VES data along Traverses 2

Figure 9a Faults/Fracture system at Nnam Alok, a shallow-CPD environment from 2D imaging result
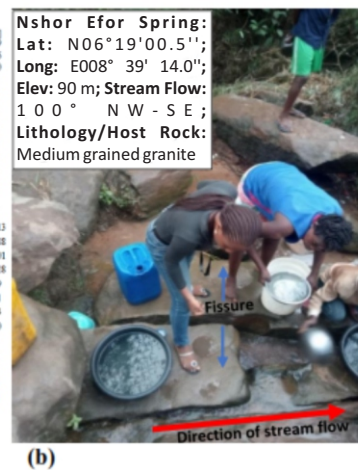
Figure 9b Faults/Fracture system at Nnam Alok, a shallow-CPD environment from site pictures at Nshor Efor Spring.

Fault zones, as well, typify basement environments of Ikom, North of Ugbodo and Northwest of Ogoja, have short wavelength responses of surface localized bodies emanating from the basement and adjacent low magnetic reliefs. Varying short and long wavelength anomalies were observed from structures created from Santonian tectonic and Albian magmatic deformational episodes, the parent events which have initiated most structures.

Spectral Analysis results for 35 Windows of 55 x 55 km dimension with 50% overlap (Fig. 3) are displayed in Table 1. Their respective uncertainties were also evaluated as well. Figures 4(a&b) are samples of spectral plots used to compute depths to the top of magnetic sources (z_t), which were obtained from the second slope/profile line breaks. Figures 4(c&d) show samples utilized to compute depths to the centriod of magnetic sources in the region (z_0) from the first slope. Table 1 provides extended details on computational results for other 55 x55 km windows taken across the region. The results revealed that depth to the top of the magnetic source ranges between 0.451 and 1.899 km with an average of 1.057 km. The Centroid depth ranges between 4.001 and 7.874 km with an average depth of 5.61731 km. The CPD values range from 6.15-14.19 km with an average of 10.1769 km. The estimated CPD, geothermal gradients, and heat flow, were obtained by applying centroid method for the blocks or windows. Figure 5a shows CPD variations and the shallowest parts are less than 8 km in the Central and Eastern parts of the study area. These areas are around Enugu, Okposi, Awgu and Obudu and Mamfe regions of the Calabar flank. On the other hand, the maximum values are located at Abakaliki, Apiapum, Okigwe axis and the bottom depths of these magnetic sources were estimated through the CPD, which gives insight to the thermal structure of the region. Average crustal temperature from lithospheric thermal condition seems to influence Curie temperature depths. Results from CPD show that high geothermal areas and volcanic environments have shallow depths <10 km. The shallow CPDs obtained around Ugbodo, Awgu, Obudu regions can be attributed to basaltic intrusives and outcropping igneous rock basements in the region which typify

volcanic arcs, ridges and elevated volcanics/extrusives. The anticlinuous Abakaliki has a higher CPD value >10 km, Apiapum and Okigwe all have high CPDs. This could be because of associations of depocenters to these regions. The geothermal gradient results were obtained utilizing the Curie-point (θ) for magnetite (580 ^{O}C)with an average thermal conductivity of 1.80 Wm^{-1} k^{-1} (Onuoha and Ekine 1999) for sedimentary shale formation and 2.5 Wm^{-1} k^{-1} (Manea and Manea, 2011) for regions with older hard rocks in the Calabar flank. The geothermal gradient values range from 20.3°C/km to 50.0°C/km with an average of 34.33°C/km and corresponding heat flow values of between 34.9 and 105 mW/m^2 with an average of 68.85mW/m^2. Figures 5a&b show variation of CPD and geothermal gradient values respectively. The geothermal gradient values increase with reduction in curie point depth.

There is inverse relationship between geothermal gradient and curie point depth as observed by Manea and Manea, 2011 and shows that shallow CPDs are generally characteristic of volcanic arcs. CPD >10 km at Abakaliki–Apiapum environs delineate possible bottom of the volcanic rocks in the region. Corroborating this, Obiora and Charan (2010) identified basaltic and doleritic sill structures including volcanic intrusives at the Abakaliki region. The Albian volcanic regions of the Calabar flank and the upper Southern Benue Trough have high heat flow and geothermal gradients, which correspond to volcanic and metamorphic regions since these two units have high heat conductivities. Geologic conditions and lithology type influence high heat flows obtained in an area. The Southern Benue Trough which predates the mid-Santonian deformation, magmatism in the Trough, silting up of 9-12 km thick sediments of the Anambra Basin (Nwajide, 2013) significantly increases heat flow (>72 mW/m^2) and geothermal gradients (>35°C/km) around these areas, by conductive heat flow via fracture conduits and diagenetic processes in over pressured zones. Two geothermal ring zones were delineated in the study area (see Fig.5b) which reveals N-S trending ring zones, North of Okposi town in Ebonyi State and E-W trending ring zones North of Mamfe and South of Obudu towns in Cross River State. Heat flow is a yardstick to the

measurement and occurrence of geothermal reserves because heat flow >88 mWm^{-2} imply an anomalous geothermal occurrence in the subsurface (Sharma, 2004). Going by established fact of threshold for mean heat flow at Continental and Oceanic crusts occurring at 65 mW/m^2 and 101mW/m^2 respectively, for good geothermal reservoirs in the area, thresholds of CPD <10 km, GG >42°C/km and heat flow >88 mW/m^2 have been established. Based on this, the study area reveals anomalous heat flow in environs of Ezzagu (Ogboji), Amanator-Isu, Azuinyaba, Nkalagu, Amagunze, Nta-Nselle, Nnam, Akorfornor, which serve as good geothermal reserves.

3D Inversion Modelling Results from Geothermal Areas

Geothermal gradient map of Figure 5b was sectioned into parts A and B as represented in figure 6. The window dimensions of A and B were extracted from the geomagnetic anomaly map earlier presented and used for magnetic vector inversion modeling procedure to reveal subsurface imaging results (Figs 7a&b). Part A of the geomagnetic anomaly field data covered in 55 x 55 km window shows sub-surface imaging results in Figure 7a. The same is applicable to the inversion results from Part B of the geomagnetic anomaly field data of same window dimension. Magnetic inversion of RTE-TMI map (Figure 3) was used to mirror magnetic models beneath anomalous geothermal fields. Models reveal deposits at varying depth of occurrences. Figure 7a shows sub-surface occurrences between 100 m asl and 9900 m in a conspicuous NE-SW trend. Regions of higher geothermal gradients >45°C/km correspond to disseminated higher magmatic deposits at about 2-5 km depths towards NE while massive deposits at Okigwe environs with lower magmatic properties occurring at the Southwestern part of the study area at about 1.8 km correspond to areas with low geothermal gradient of 21.2°C/km (Fig.7a). Figure 7b reveals the subsurface imaging results from Part B obtained from geomagnetic anomaly field data. There are a lot of models obtained from this section. Most of the models have high magnetic intensities and are quite surficial as seen occurring at the extreme North to Northwest and South to Southeast. Surficial to intermediate

deposits on the average occur between depths of about 150 m to 4500 m while the rest occur as deep as >9500 m. There is a visible NW-SE trend in the pattern of occurrence of these deposits around environs cross-cutting South of Ikom, almost at the central part of B, Northwest and West of Ikom, North, Northeast and Northwest of Obubra and Ugbodo. Figure 7b reveals a lot of models obtained from this window size, Most of the models of high MVI values denote deposits with more magnetic properties because of very high corresponding residual anomaly responses (when compared with Fig.3), and they are almost surficial going by their depths of occurrences between <100 m to <5 km as corroborated from shallow CPDs <10 km depth. There are both shallow and deeper occurrences of some of the deposits. This is most likely caused by stress fields from Charcot fault systems, accompanied by igneous activities that pre-date the Santonian deformational regime. Albian and early Cenomanian fractured basements which have possibly resulted from this phenomenon and overlain by silted Odukpani and Asu River Group (ARG) sediments provide migration pathways for intrusives, hydrothermal fluids and heat flow.

Evaluation of Models Influencing Geothermal Energy Resource from Field Results

Two (2) VES results (Figs.8 a&b) from Nnam Alok were obtained along profile directions of 125° and 035° from first and second traverses respectively. It is observed that within the vicinity of Alok delineated as having high potential for geothermal resource, there occurs near-surface emplacement of basement rocks with little shale stringers sitting on top of the basement. This can be encapsulated that a befitting model of the proposed geothermal resource in this area is the Hot Dry Rock (HDR) model. Thermal subsurface heat sources, 500 m or less, produce measurable thermal anomalies at the surface and thermal anomalies due to local subsurface heat sources are impossible to detect at the surface or at depths of only a few feet (Lovering and Goode, 1963) except by examining drilled hole temperatures. Nevertheless, diurnal effects, time and weather of the day, time of the year, thermal property and surface temperature of granite rock from sun's heat, local heat sources such as an oxidizing

sulphide or conductive mineral body suspected to be barite, as observed from occurrence of material resistivity >1000 Ωm (Akpan *et al.,* 2014; Obi *et al.,* 2014) within fractured shale at depth of 5-15 m}, may play a role in temperature change. Some of the lower resistivity values at 15-45 m, shallower than undifferentiated basements, indicates partly weathered/fractured basements, and the fracture could be extensive and have possibly aided subsurface heat flow across these environs.

Considering the location of Nshor Efor Spring in anomalous geothermal environment, it was visited in the morning to ascertain the temperature of the water which recorded a temperature lower than normal body temperature of 37°C. However there is usually a dramatic increase in temperature of water in early morning hours of the raining season to as much as 42°C, which is a clear indication of an abnormal temperature and can be considered a surface manifestation of temperature variations in the subsurface. The fault system delineated below creates preferred pathways for subsurface-surface circulation of geothermal fluids and heat flow.

CONCLUSION

The aeromagnetic TMI map of parts of the Southeastern Nigerian sedimentary basin was reduced to the equator and subjected to magnetic vector inversion and spectral analysis with a view to estimating depths to magnetic tops (Z_t), base of the magnetic layer (curie point depth) and the geothermal energy heat flow as a means of evaluating the geothermal energy resource. The study also utilised 1D vertical electrical sounding and 2D imaging techniques to investigate the influence of fracture system as pathway to heat flow.

Results from spectral analysis show depths to the top of the magnetic source ranging between 0.45 and 1.90 km with an average of 1.06 km; centroid depth of 4 - 7.87 km with an average of 5.61 km and Curie Point Depth (CPD) of between 6.15 and 14.19 km with an average of 10.18 km. CPD was used to estimate geothermal gradient values which range from 20.3°C/km - 50.0°C/km with an average of 34.33°C/km and corresponding heat flow values of 34.9 - 105 mW/m^2 with an average of 68.85 mW/m^2 utilizing an average

thermal conductivity of 2.15 Wm^{-1} k^{-1}.

Ezzagu (Ogboji), Amanator-Isu, Azuinyaba, Nkalagu, Amagunze, Nta-Nselle, Nnam, Akorfornor environs are situated within regions of high geothermal gradients (>38°C/Km) and models delineated beneath these regions using 3D Magnetic Vector Inversion, having dominant NW-SE and NE-SW trends at shallow to greater depths of <1 km to >7 km bsl. Based on VES and 2D imaging models the geothermal system in Alok can be classified as Hot Dry Rock (HDR) type, which may likely have emanated from fracture systems. It can be concluded that the study area has prospect for geothermal energy development.

REFERENCES

Abraham, E. M. and Nikitnam, E. E. 2017. Review of geothermal energy research in Nigeria: The Geoscience Front. *International Journal of Earth Science and Geophysics,* 3: 015, 1 – 10.

Akande, S.O; Hoffknecht, A. and Erdtmann, B.D. 1992. Rank and petrographic composition of selected upper Cretaceous and tertiary coals of Southern Nigeria. *International Journal of Coal Geology,* 20, 209-224.

Akanbi, E-M and Udensi, E.E. 2006. Structural trends and spectral depth analysis of the residual field of Pategi Area, Nigeria, using aeromagnetic data, *Nigerian Journal of Physics,* 18(2), pp.271-pp.276.

Akpan, A.E; Ebong, D; Ekwok, S.E and Joseph, S. 2014. Geophysical and Geological studies of the spread and industrial quality of Okurike baryte deposit. *American Journal of Environmental Science,* 10(6): 566-574.

Azaiez, H.; Gabtni, H.; Chabaane, A.; Sayem, G. and Bedri, M. 2020. Geophysical study of Hanimam Sidi Maamar geothermal site in Central Tunisia for sustainable development. *Journal of African Earth Sciences.* https://doi.org/10.1016/j.jafrearsi.2020.103897.

Beardsmore, G. R. and J. P. Cull. 2001. CrustalHeat Flow: A Guide to Measurement and Modelling.New York, NY:Cambridge University Press. Abstract) 7. ASEG-PESA Conference, Melbourne. (Chapter7).

Benkhelil, M. J. 1989. The origin and evolution of the Cretaceous Benue Trough, Nigeria. *J.Afric. Earth Sci.*, 8, 251-282.

Bhattacharyya, B.K.and Leu, L.K., 1975a. Analysis of magnetic anomalies over yellow stone national park: mapping and curie point isothermal surface for geothermal reconnaissance. *J. Geophys. Res.* 80, 4461–4465.

Bhattacharyya, B.K.and Leu, L.K., 1975b. Spectral analysis of gravity and magnetic anomalies due to two-dimensional structures. *Geophysics,* 40, 993–1013.

Blakely, R.J 1995. Potential Theory in Gravity and Magnetics Applications, Cambridge. University Press, Cambridge 464.

Donny, W. R.; Djeli, A. T. and Cyrke, A.N.B. 2020. Geothermal gradient and subsurface temperature for estimation of sources, patterns and heatflow directions in hydrothermal area of Minahasa, Indonesia. *Journal of Critical Reviews,* 7(5),905-907.

Chabaane, A.; Redhaounia, B.; Gabtni, H. 2017. Combined application of vertical electrical sounding and 2D electrical resistivity imaging for geothermal groundwater characterisation: Hammam Sayala Hot Spring case study (NW Tunisia). *Journal of African Earth Sciences*, 134, 292 – 298. http://dx.doi.org/10./ 016/j.jafrearsci. 2017.07.003

El-Qady, G. 2006. Exploration of a geothermal reservoir using geoelectrical resistivity inversion; case study of Hammam Mousa, Sinai, Egypt. *J. Geophysics. Eng.* 3, 114 – 121 doi. 10.1088/1742 –2132/3/2/002.

Fatoye, F.B.; Ibitomi, M.A. and Omada, J.I. 2014. Lead-Zinc-Barytes mineralization in the Benue Trough, Nigeria: Their geology, occurrences and economic prospective. *Advances in Applied Science Research*, 5(2), 86-92.

Georgsson, L.S. 2013. Geophysical methods used in geothermal exploration. Paper presented at Short Course VIII on Exploration for Geothermal Resource. Organised by (UNU – GTP, GDC and KenGen, at Lake Bogoria and Lake Naivasha, Kenya. Oct. 31 – Nov. 22, 2013.

Hoover, H.C. and Hoover, L.H. 1556. Georgius Agricola *De Re Metallica* translated from the first Latin edition of 1556. New York: Dover, 1912; reprinted 1950.

Hsien-Hsiang, H.; Chieh-Hung, C.; Pei-Ying, L and Horng-Yuan, Y. 2014. Curie point depth from spectral analysis of magnetic data in Taiwan. *Journal of Asian Earth Sciences*, 90, 26-33.

International Geothermal Association (IGA). 2020 .Geothermal outlook in East Africa: Perspective for Geothermal Development. (Presentation by P. Omenda, Director IGA; Consultant). htpps://www.irena.org/publications/20 20/Nov/Geothermal-Development-in-Eastern-Africa.

Kana, J.D.; Djongyang, N.; Raidandi, D.; Nouck, P.N. and Dadje, A. 2015. A review of geophysical methods for geothermal exploration. *Renewable and Sustainable Energy Reviews*, 44, 87-95. http://dx.doi.org/10.1016/j.rser.2014.12.026.

Kendall, A.C. 1984. Evaporites. In: Walker, R.G (ed.). Facies models: Geoscience Reprint Series 1, New foundland, Canada, Geological Association of Canada, 259-296.

Korhonen, J.V. 2005. Airborne Magnetic Method: Special Features and Review on Applications. Geological Survey of Finland, Paper 39, 77–102.

Ladipo, K.O. 1988. Paleogeography, sedimentation and tectonics of the upper cretaceous and tectonics of the upper cretaceous Anambra Basin, Sotheastern Nigeria. *Journal of African Earth Sciences* 7, 865-871.

Li, Y. 2017. From susceptibility to magnetization: *Advances in the 3D inversion of magnetic data in the presence of significant remanent magnetization*, paper, 18, 239-pp.260.

Li, Y.; Shearer, S.; Haney, M. and Dannemilller. 2010. Comprehensive approaches to the inversion magnetic data affected by remanent magnetization: *Geophysics*, 75, 1-11.

Lovering, T.S and Goode, H.D. 1963. Measuring geothermal gradients in drill holes less than 60 feet Deep East Tintic District,

Utah Washington: United States Government Printing Office.

Lowrie, W. 2007. Fundamentals of Geophysics Cambridge: Cambridge University Press, New York.1st, edition.

Maden, N. 2010. Curie-point depth from spectral analysis of magnetic data in Erciyes stratovolcano (Central TURKEY). *Pure Appl. Geophys.* 167, 349–358.

Manea, M.and Manea, V. C. 2011. Curie point depth estimates and correlation with subduction in Mexico. *Pure and Applied Geophysics*, 168, 1489. https://doi.org/10.1007/s00024-010-0238-2.

Nigerian Geological Survey Agency 2010. Digitized map of the geology of Lower Sedimentary Basin from geologic map of Nigeria.

Nwajide, C.S. 2013. Sequence Stratigraphy of the Lower Benue Trough in Geology of Nigeria's Sedimentary basin. Published by CSS Bookshop limited.pp.287.

OAK GROUP.2013. Hydrogeophysical Investigation for the evaluation of geothermal potential beneath the premises of OAK Group, Isheri, Ogun State. Technical Report 45 pp.

Obaje, N.G. 2009. Geology and Mineral Resources of Nigeria. Springer Dordrecht Heidelberg London New York, 2009.

Obi, A.A; Ekwueme, B.N and Akpeke, G.B. 2014. Reserve estimation of barite deposits using geologicaland geophysical investigation, in Cross River, Southeastern Nigeria, *Journal of Environmental Earth Science,* 4(10): 16-31.

Obiora, S. C., and Charan, S. N. 2010. Tectonomagmatic origin of some volcanic and sub-volcanic rocks from the Lower Benue rift. Nigeria. *Journal African Earth Sciences.*, 58, 197–210.

Odoma, A.N.; Obaje, N.G.; Omada, J.I.; Idakwo, S.O. and Erbacher, J. 2013. Paleoclimate Reconstruction During Maamu Formation (Cretaceous) Based on Clay Mineral Distributions. IOSR *Journal of Applied Geology and Geophysics* (IOSR-JAGG). e-ISSN: 2321–0990, p-ISSN: 2321–0982.1(5), 40-46.

Okiyi, I.M., Selemo, A.I.; Ibeneme, S.I.;

Olorunfemi, M.O and Adikwu, S.A. 2021. Estimation of Lineaments and structures as indices of mineralization in parts of southeastern Nigerian Sedimentary basin of Nigeria. *Journal of Earth and Atmospheric Research.* (In Press).

Okubo, Y., Graf, R.J., Hansen, R.O., Ogawa, K. and Tsu, H. 1985. Curie point depths of the island of Kyushu and surrounding areas, Japan. *Geophysics* 50, 481–494.

Onuoha, K. M., and Ekine, A. S. 1999. Subsurface temperature variation and heat flow in the Anambra Basin, Nigeria. *Journal of African Earth Sciences,* 28(3), 641–652.

Opara, A.I. 2011. Estimation of the depth to magnetic basement in parts of the Dahomey Basin, Southwestern Nigeria. *Australian Journal of Basin and Applied Sciences, 5(9), 335-343.*

Perry, J. 1895a. On the Age of the Earth: *Nature,* 51, 224-227.

Perry, J. 1895b. On the Age of the Earth: *Nature,* 51, 341-342.

Perry, J. 1895b. On the Age of the Earth: *Nature,* 51, 582-585

Petters, S.W. 1978. Stratigraphic Evolution of the Benue Trough and Its Implications for the Upper Cretaceous Paleogeography of West Africa. *The Journal of Geology.* 86(3), 311–322.

Pilkington, M. 2009. 3-D msgnetic data space inversion with sparseness constraints: Geophysics, 7, 7-15.

Pilkington, M and Bardossy, Z. 2015. DSIM3D: Software to perform unconstrained 3D inversion of magnetic data. Geological Survey of Canada, Open File 7749, 1.zipfile.doi:10.4095/295611.

Ravat, D.; Pignatelli, A.; Nicolosi, I. and Chiappini, M. 2007. A Study of spectral methods of estimating the depth to the bottom of magnetic sources from near surface magnetic anomaly data. *Geophysical Journal International,* 169(2): 421-434.

Reijers, T. J. A. & Nwajide, C.S. 1998. Geology of the Southern Anambra Basin. Unpublished Report for Chevron Nigeria Limited. Field Course Note, pp.66.

Reynolds, R.L.; Rosenbaum, J.G.; Hudson, M.R. & Fishman, N.S. 1990. Rock magnetism, the distribution of magnetic minerals in the

Earth's crust, and aeromagnetic anomalies. *United State Geological Survey Bulletin,* 1924, 24-25.

Ryan, Carbotte, Coplan, O' Hara, Melkonian, Arko, Weissel, Ferrini, Goodwillie, Nitsche, Bonczkowski & Zemsky. 2009. Topographical Map of the Study Area. Multi-Resolution Topography Synthesis, Geochem. Geophys. Geosyst..

Shah, M.; Sircar, A.; Vaidya, D.; Sahajpal, S.; Chaudhary, A. and Dhale, S. 2015. Overview of Geothermal Surface Exploration Methods. IJARIIE – ISSN (0) – 2395 – 4396, 1(4), 55 – 64. (www.ijariie.com)

Sharma, P. V. 2004. Environmental and engineering geophysics (p. 475). Cambridge: Cambridge University Press.

Shearer, S. 2005. Three dimensional inversion of magnetic data in the presence of remanent magnetization: MSc. thesis, Colorado School of Mines and 74th Annual International Meeting, SEG, Expanded Abstracts, pp.774-pp.777.

Shuey, R.T.; Schellinger, D.K.; Tripp, A.C. and Alley, L.B. 1997. Curie depth determination from aeromagnetic spectra: *Geophysical Journal of the Royal Astronomical Society.* 50, 75-101.

Spector, A. & Grant, F.S. 1970. Statistical Models for Interpreting Aeromagnetic Data. *Geophysics,* 35, 293-302.

Stampolidis, A., Kane, I., Tsokas, G.N., Tsourlos, P. 2005. Curie point depths of Albania inferred from ground total field magnetic data. *Surv. Geophys.* 26, 461– 480.

Tanaka, A.; Okubo, Y. & Matsubayashi, O. 1999. Curie Point Depth based on Spectrum Analysis of the Magnetic Anomaly Data in East and South East Asia. T*ectonophysics* 306, 461-470.

Tissot, B.P and Welte, D.H. 1978. Petroleum formation and occurrence: A new approach to oil and gas exploration, XVIII +5385, 241 Abb., 70 Tab. Berlin-Heidelberg-New York1978. Springer-Verlag. DM 7900.

Turcotte, D.L. and Schubert, G.1982. Geodynamics. Cambridge University Press, New York.

Utsugi, M. 2019. 3D Inversion of magnetic data based on L_1-L_2 norm regularization. *Earth,*